PHYSICAL REVIEW D VOLUME 16, NUMBER 7 1 OCTOBER 1977

Results on $\pi^+\pi^- \to \pi^0\pi^0$ cross section from peripheral dipion production in the reaction $\pi^- p \to \pi^0\pi^0 n$ at 2.01 GeV/c

M. David, G. Villet, R. Ayed, P. Bareyre, P. Borgeaud, J. Ernwein, J. Feltesse, Y. Lemoigne, and A. V. Stirling
Département de Physique des Particules Elémentaires, CEN-Saclay, France
(Received 1 June 1976; revised manuscript received 26 October 1976)

We report results on $\pi^+\pi^- \to \pi^0\pi^0$ total and differential cross sections from threshold to 1.1-GeV $\pi\pi$ mass. These results have been obtained from a high-statistics experiment studying the reaction $\pi^- p \to \pi^0\pi^0 n$ at 2.01 GeV/c incident π^- momentum with the Chew-Low extrapolation method. The π^0's have been detected and their momenta analyzed in a large-gap cylindrical spark chamber placed in a magnetic field. The results show three salient features: (i) A large $I = 0$ production with $\sigma_{\text{tot}}(\pi^+\pi^- \to \pi^0\pi^0)$ approaching the S-wave unitarity limit in the 550–750-MeV $\pi\pi$ mass region, without any narrow structure. (ii) A slow fall of $\sigma_{\text{tot}}(\pi^+\pi^- \to \pi^0\pi^0)$ in the region of 750–950-MeV $\pi\pi$ mass. This feature is not predicted by the "down" solution for the $I = 0$ S-wave $\pi\pi$ phase shift which has been reported recently. (iii) The presence of D-wave effects above 850 MeV as indicated by our extrapolated angular distributions.

I. INTRODUCTION

A great deal of theoretical and experimental work has been done in the study of $\pi\pi$ scattering. So far most results have been obtained from peripheral dipion production ($\pi^+\pi^-$ or $\pi^-\pi^0$) in pion-nucleon collisions. From the beginning these experiments have shown the well-known $L = 1$, $I = 1$ wave (P_1): the ρ resonance of the $\pi\pi$ system at a mass around 765 MeV.

In order to extract the other waves ($S_0, S_2, D_0, D_2, F_1, \ldots$), one needs not only to know the peripheral dipion production but also to perform a Chew-Low extrapolation giving on-mass-shell data which allow a phase-shift analysis of total cross sections and angular distributions. With this method, in spite of a large amount of data in the 3 final states ($\pi^+\pi^+, \pi^-\pi^0, \pi^+\pi^-$), one cannot obtain unambiguous partial waves, mainly for S_0.

To determine this wave, another approach consists in using data of peripheral $\pi^0\pi^0$ production. In this case the phase difference $|\delta_{S_0} - \delta_{S_2}|$ is determined directly. Unfortunately, the reactions

$$\pi^- p \to \pi^0\pi^0 n \tag{1}$$

and

$$\pi^+ n \to \pi^0\pi^0 p \tag{2}$$

or

$$\pi^+ p \to \pi^0\pi^0\Delta^{++}$$

are difficult to study experimentally because neutrals have to be detected (γ rays, neutrons, or both). These experimental difficulties can explain why there is no general agreement among the different experiments.

In this paper we report results on a study of reaction (1) at 2.01 GeV/c. Preliminary results on this subject were reported at the Tallahassee Meson Spectroscopy Conference (1973) and at the Aix-en-Provence International Conference (1973).[1] In the present work we have included more information about background reactions and a better determination of the detection efficiency.

In this experiment, the neutron was not detected. In order to obtain enough constraints to fit reaction (1), we put our efforts on a clean identification of the γ rays and on the best possible accuracy of their energy measurement.

The apparatus had a high detection efficiency over a wide solid angle and therefore allowed us to collect events over the full range of $\cos\theta^*_{\pi\pi}$. The desired accuracy of the γ-ray energy measurement obliged us to work at a moderate P_{lab} in order to produce low-energy γ rays (i.e., $P_\gamma < 1$ GeV/c); they were detected in a large-gap spark chamber, whose electrodes were made of lead (1 mm thick) placed in a magnetic field. The experimental setup is described in Sec. II.

After scanning and automatic measurement of the tracks, we were left with 6929 4γ events. In Sec. III, we summarize the geometrical-reconstruction method, the kinematical fits, and the calculation of the efficiencies and corrections. We also describe various checks which were used to obtain a weighted sample and to evaluate the $\pi^0\pi^0$ background coming mainly from $3\pi^0$, $4\pi^0$, and N^* production.

After verifying that the extrapolated cross section was near 0 for $\Delta^2/\mu^2 = 0$, we performed a constrained Chew-Low extrapolation which yielded the total and the differential elastic cross section for $\pi^+\pi^- \to \pi^0\pi^0$ (Sec. IV).

In Secs. V and VI we compare, respectively, our results with others and with phase-shift-analysis predictions.

II. EXPERIMENTAL LAYOUT

A. General description

The apparatus was designed to study the reactions $\pi^- p \rightarrow$ neutron $+K\gamma$ ($K = 2$ to 6) and was installed near the synchrotron SATURNE. The neutron was not detected, owing to the small detection efficiency and to the difficulty of avoiding biases. An unambiguous identification of the γ rays and an accurate measurement of their momenta was therefore needed. The conventional γ detection by shower production is not well suited for this experiment because a large fraction of γ rays have a small energy (25% of γ's have $P_\gamma < 150$ MeV/c).

γ rays were detected by pair creation across thin plates of lead (1 mm thick). Their momenta were obtained from the curvature of electron trajectories inside a magnetic field. Moreover, the need of a large solid angle for γ-ray detection led to the apparatus shown on Fig. 1(a). A large-gap

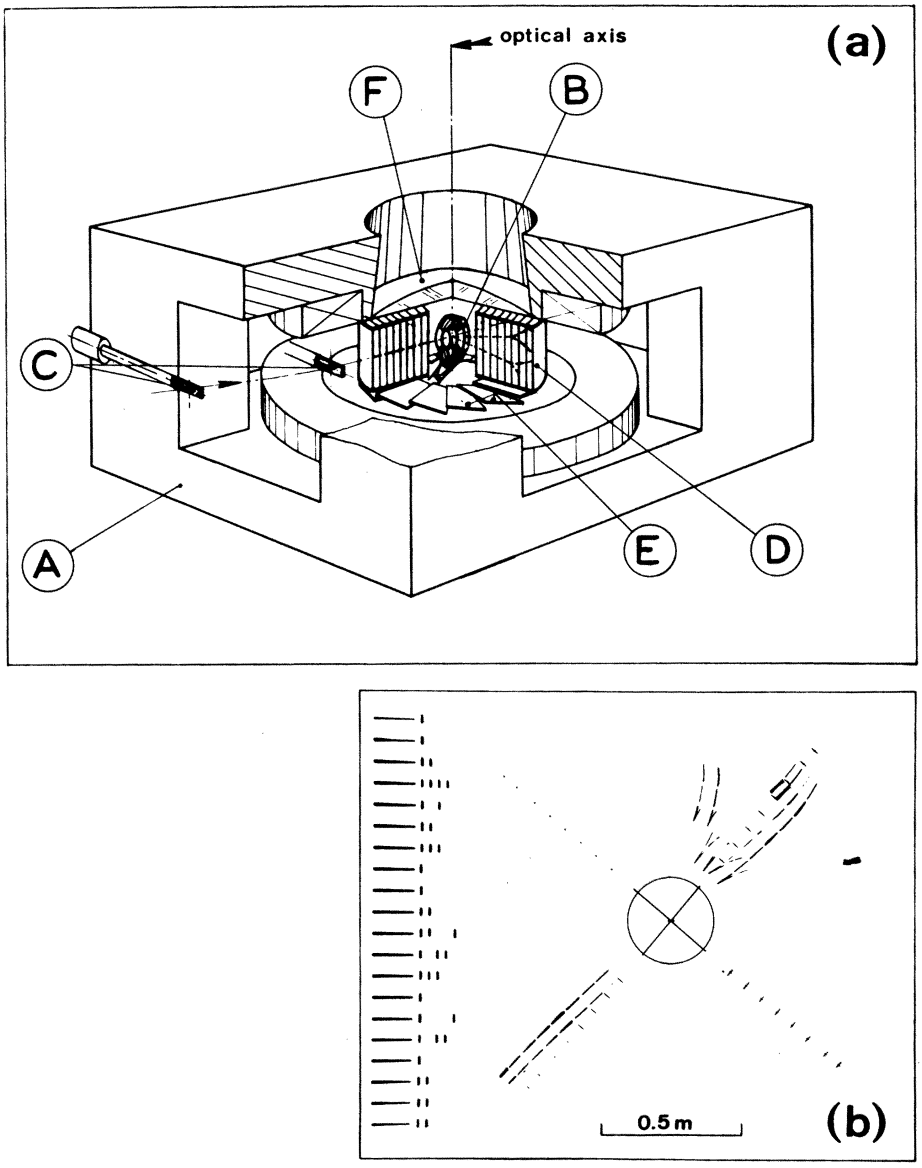

FIG. 1. Facility perspective of the experimental layout: (a) A, "Goliath" magnet, B, H_2 liquid target and anticounters, C, beam counters, D, cylindrical wide-gap spark chamber, E, fan-shapped mirror assembly for stereoscopic photography, F, field lens of 7 meters focal length. (b) A typical 4-electron-pairs event as recorded on film. Note the direct and reflected (shifted anticlockwise) sparks images.

cylindrical spark chamber (D) was immersed in the magnetic field (1.8 T) of a large magnet "Goliath" (useful volume 2 m in diameter and 0.9 m in height). The spark chamber surrounded a liquid hydrogen target (10.7 cm long). A set of counters (B) allowed us to trigger only on neutral reactions with all γ rays emitted in the solid angle (5.1 sr) covered by the chamber. A system of 14 tilted mirrors (E) provided the small stereoscopic angle (8°) required by the cylindrical geometry of the chamber. The direct and reflected sparks were focused onto a camera by a 1.75-m diameter field lens of 7-m focal length (F). A typical 4γ event recorded on the film is shown on Fig. 1(b).

A double-focusing pion beam was collected at 0° from an external target of the synchrotron SATURNE. At 2.01 GeV/c the average beam intensity was 3×10^4 pions per spill (350 msec) with a momentum dispersion of $dp/p = \pm 0.015$.

B. Specific features of the apparatus

1. The chamber

The cylindrical wide-gap spark chamber (useful volume 1.60 m in diameter and 0.7 m in height) was made of 9 concentric electrodes (1-mm lead), sandwiched between 0.5-mm aluminum foils; the last lead plate, however, was 3.3 mm thick. The gap was 7 cm and the inner electrode had a radius of 20 cm. The high-voltage pulse (225 kV, rise-time 40 nsec and width 20 nsec) was delivered by a Marx generator and applied to the chamber on the middle electrode.

In this type of chamber, the sparks follow the trajectories of charged particles if the angle with the electric field is less than 35°. This condition is satisfied by pair-creation electrons in the first few gaps after the electrode of conversion, due to the geometry of the anticounter and to the position of the target.

The memory of the spark chamber was reduced to 2 μsec by addition of 3×10^{-4} volumes of Freon in the gas mixture. The percentage of pictures with "old tracks" (mostly beam tracks) was thus less than 10%. In addition, about 7% of the pictures show a "young" beam track which crossed the chamber during the time delay necessary to trigger the spark chamber ($\simeq$600 nsec). In such a chamber, spurious sparks are very rare and can by no means be confused with charged-particle tracks.

In the case of γ-ray detection by pair creation, the energy distribution of the electrons is quite flat, so that a certain fraction of the γ rays were seen with only the track of the most energetic electron, the other being stopped in the electrode. A small percentage ($\simeq$3%) of single tracks came from the Compton effect. Both effects account for the fact that 48% of the γ's were detected as single-electron tracks. However, this single-electron track given by a γ ray cannot be confused with a primary charged track mainly because of the empty gaps between the target and the materialization apex, the great curvature of the trajectories, or the characteristic bremsstrahlung along the track. Electrons escaping from an electrode with an energy as low as 10 MeV have been detected, but the automatic measurement device imposed a cut at 20 MeV corresponding to a radius of curvature less than 4 cm.

This chamber had a very good efficiency for events with very high multiplicities but there was a large range in the spark luminosity.

2. The optics

With the cylindrical geometry and the opacity of the electrodes of the chamber, it was not possible to take two photographs with a 90° stereoscopic angle.

The height coordinate z in the chamber was obtained in the following manner: In addition to the direct image of the spark, a reflected image was given by mirrors assembled in the form of a fan underneath the chamber and was recorded on film. The distance between these two images is roughly proportional to the height z. The number of mirrors (14) and the angle ($\alpha = 4°$) resulted from a compromise between the wanted z precision, the volume available below the chamber, and the interference of the rays with cylindrical electrode structures.

The field lens was made of glycerine inserted between a Lucite plane, 24 mm thick, and a portion of Lucite sphere, 8 mm thick. The curvature was obtained by blowing a heated plate. Water was added to the glycerine in order to obtain a refractive index equal to the index of the Lucite envelope.

3. The counters

In order to eliminate most of the accidental tracks, the incident π^- was defined by means of four scintillation counters located along the trajectory of the beam. The last counter, placed only 3 cm in front of the target, was located directly inside the vaccum vessel. Also located in this vessel, and all around the target, were two counters made of lead-scintillator sandwiches. The aim of these counters was to reject processes with a scattered charged particle as well as the neutral scattering processes where γ rays are emitted outside the useful volume of the chamber.

The photomultipliers were placed outside the magnet at the end of long Lucite pipes (3 m) to preserve them from the strong magnetic field. They were shielded to avoid the effect of the fringing field (about 300 G).

III. DATA ANALYSIS

A. Scanning of the γ-ray multiplicities

A large-gap spark chamber detecting γ rays of low energy by pair conversion permits a clear identification and gives a good measurement of their kinematical parameters. Nevertheless there exist two main sources of spurious γ rays:

(i) γ rays of bremsstrahlung emitted in the forward direction by the electrons crossing a lead electrode can be converted downstream.

(ii) Some electrons escaping from the chamber can re-enter it because of the curvature of the trajectories in the magnetic field.

At the scanning level, the γ-ray multiplicities were recorded without distinction between primary and spurious γ rays. For each event including 3 or more primary γ-ray candidates (47 000 events) the scanner measured 3 points per direct and reflected electron tracks. This procedure was needed to help the track-finding program which was complicated because of the high number of tracks per picture (a 4γ-ray event showed an average of 14 direct and reflected tracks).

In order to check the scanning efficiency, 10 000 pictures were scanned a second time by physicists. A discrepancy in the γ-ray multiplicities appeared and was mainly due to tangled topologies. A complete treatment of the events coming from the second scanning showed that only the normalization was affected and not the $\pi^0\pi^0$ mass spectra or the angular distributions. This effect was removed in the final analysis by applying a correction of 19% in the normalization.

B. Measurement and geometry

To make use of the continuous trajectories and to gain sufficient information for short tracks, it was necessary to make one measurement every centimeter. This requirement and the large number of events to be measured made it necessary to use an automatic measurement device ARIANE II.[2]

ARIANE II is a flying-spot cathode-ray tube controlled by a small on-line computer (CDC 8090) which reads the data box and digitizes the sparks (7 points per gap) and the fiducial marks. The average measuring precision corresponds to 0.1 mm in real space with a measuring time of 30 sec per frame.

With the help of the rough measurements done at the scanning level, the track-following and the matching between direct and reflected trajectories have been done with an efficiency of 98.5%

A parametrization of the optics (field lens and tilted mirrors) was necessary to determine the transformation between measured points on the film and real-space coordinates in the whole volume of the chamber (diameter = 1.6 m, height = 0.7 m). In order to obtain the parameters of this transformation, a horizontal grid was photographed at different levels (z) inside the magnet before and after each data-taking. The global uncertainties on point reconstruction in space were: $\sigma_x = \sigma_y = 0.65$ mm (in the horizontal plane perpendicular to the magnetic field) and $\sigma_z = 7.0$ mm.

C. $e^{\pm}$ and γ kinematic parameters and filter program

Each time an electron crosses a 1.0-mm-thick lead electrode, it suffers an energy loss by bremsstrahlung. This loss is highly non-Gaussian.[3] The most probable loss ($\Delta E/E = 0.02$) is very different from the average loss ($\Delta E/E = 0.17$), hence the variance is large ($\pm 14\%$). As we wanted to determine the energy of the electron by fitting a cyclindrical helix assuming a uniform magnetic field and a relatively negligible energy loss, the useful track length was limited to 3 gaps (i.e., 21 cm). For trajectories with a sudden jump of curvature across an electrode, the track length was limited to its upstream portion.

Knowing the geometrical parameters of the electron trajectories, we computed the directions of the parent γ rays and used them to eliminate the spurious tracks mentioned above:

(1) When the assumed parent γ ray did not point toward the target, the track was considered as a re-entering electron and was rejected.

(2) Taking into account the peaked angular distribution of the bremsstrahlung $\sigma_{\theta\ \mathrm{rad}} = 0.67(M_e/E_e)\ln(E_e/m_e)$ (for instance $\sigma_{\theta\ \mathrm{rad}} = 1.0^\circ$ for a 100-MeV electron), converted bremsstrahlung γ rays were eliminated in the following way: For each electrode crossed, the tangent to the trajectory was computed. Any downstream electron located inside a cone centered on the tangent with an aperture proportional to $\sigma_{\theta\ \mathrm{rad}}$ and to the experimental angle error was removed.

In order to obtain the true energy of the electrons, several corrections were applied to the visible momentum:

(i) For all tracks the momentum was increased by 8.5%, which corresponds to the average energy loss in the conversion electrode.

(ii) A variable correction depending on the lead thickness crossed by the electron after the con-

version electrode was also applied.

(iii) In 6% of the cases a converted γ of bremsstrahlung pointed towards the origin of the parent electron; its energy was added to the primary γ-ray energy.

The momenta of the primary γ rays and their errors were obtained in the case of pairs by $\vec{P}_\gamma = \vec{P}_{e^-} + \vec{P}_{e^+}$ and in the case of a single electron by $\vec{P}_\gamma = \vec{P}_e + 20$ MeV $(\vec{P}_e/P_e)$, the last term being the average momentum of the unseen electron.

The vertex was calculated by a least-squares-fit method using the extrapolated trajectory of the incident pion across the target as well as the measured direction and the materialization point of the γ rays. The accuracy of this vertex determination was ± 1 cm along the pion track. This method also gave the fitted directions of γ rays and their errors which, associated with the momenta calculated above, furnish the input parameters for the kinematical fit of the reactions.

D. Kinematical fitting

The energy loss by bremsstrahlung emitted by an electron crossing a fraction of a radiation length of lead is non-Gaussian and is therefore incompatible with the variable $1/P$ which is usually used in the fitting programs where Gaussian errors are assumed. We used our 2γ-ray events where the charge exchange dominates in order to find a variable to be fitted which gives nearly a Gaussian distribution of $M_{\gamma\gamma}^2$ in the one-constraint fit of the reaction $\pi^- p \to \gamma\gamma n$. The variable $\ln P_\gamma$ (Ref. 4) (instead of the usual $1/P_\gamma$) was found to be convenient. Figure 2 displays the $\gamma\gamma$ mass spectrum at incident momenta of 757 MeV/c and 2010 MeV/c. This spectrum exhibits two peaks for π^0 and η^0, centered, respectively, at 136 MeV/c and 544 MeV/c, the average mass resolution being 15%.

All 4γ events (6929) were fitted with the $\pi^0\pi^0$ hypothesis. The assumption that γ rays came from $2\pi^0$'s and the fact that the neutron was not detected led to a 3C fit. For each 4γ event, among the three possibilities of pairing γ rays into $2\pi^0$, the combination with the best χ^2 was kept for the analysis. The average difference between the three χ^2 was 8. We have checked by Monte Carlo calculations that, for a cut at $\chi^2 < 20$, the choice of the combination with the best χ^2 was the good one in 90% of the cases. The 10% of bad pairings gave no visible effects on the distributions.

The number of events with $\Delta^2/\mu^2 < 15$ and $\chi^2 < 20$ was 2295. These events were used later to perform the Chew-Low extrapolation.

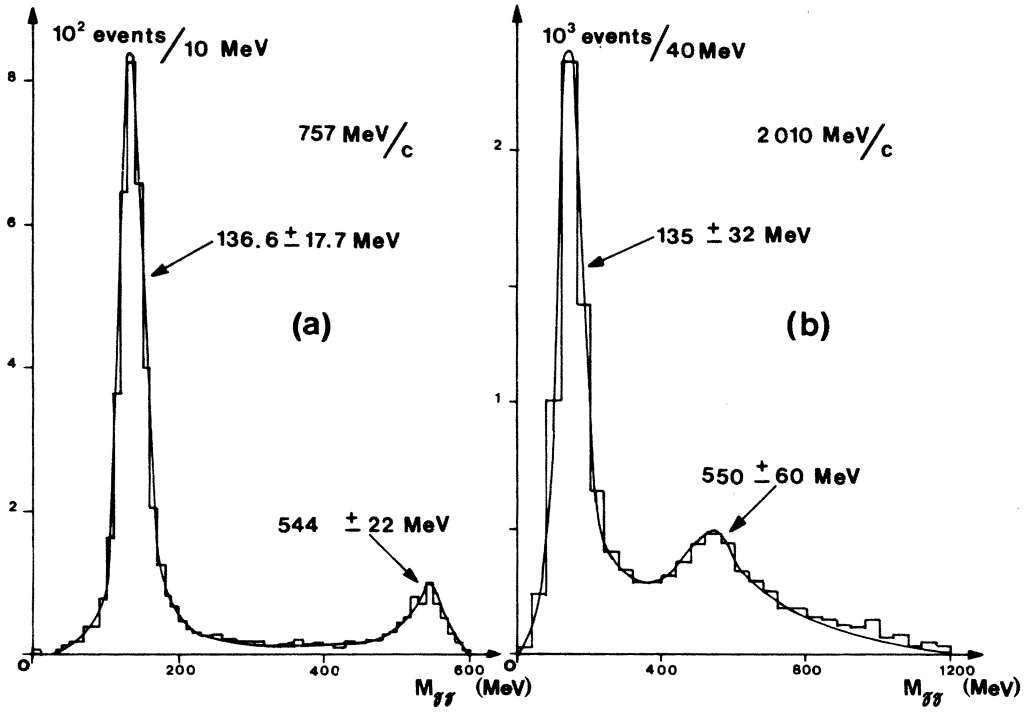

FIG. 2. $\gamma\gamma$ mass spectrum for 2γ events fitting the reaction $\pi^- p \to \gamma\gamma n$ with $\chi^2 < 5$, (a) for 757 MeV/c, (b) for 2010 MeV/c. The curves represent the Monte Carlo simulation.

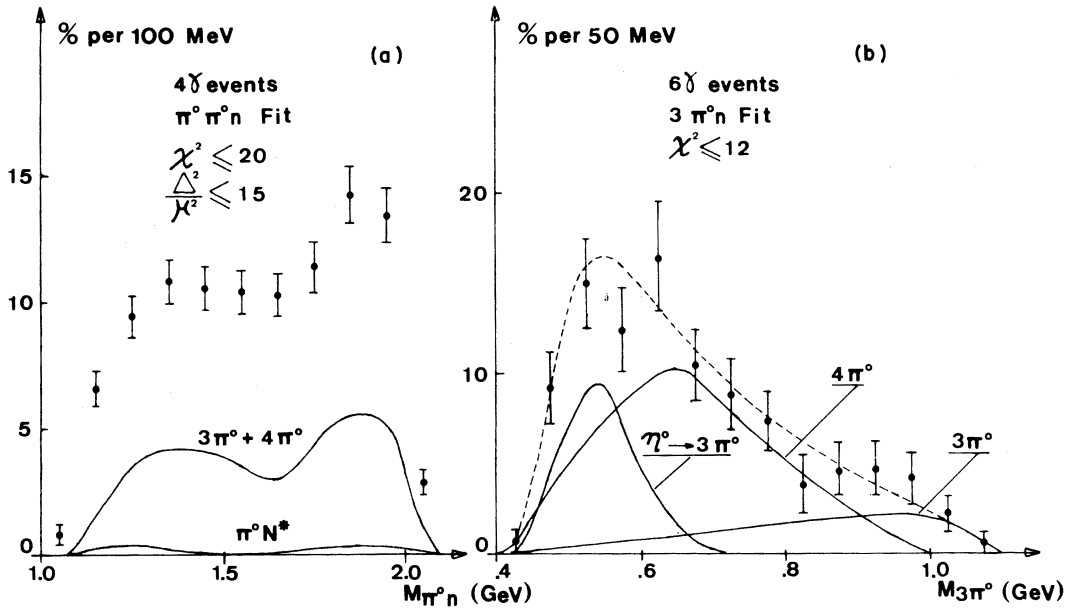

FIG. 3. (a) $\pi^0 n$ invariant-mass spectrum for experimental 4γ events fitting the reaction $\pi^- p \to \pi^0\pi^0 n$ ($\chi^2 < 20$, $\Delta^2/\mu^2 < 15$). The curves show the calculated contribution of $3\pi^0 n + 4\pi^0 n$ and $\pi^0 N^*$ events. (b) $3\pi^0$ invariant-mass spectrum for experimental 6γ events fitting the reaction $\pi^- p \to 3\pi^0 n$ ($\chi^2 \lesssim 12$). The dashed curve represents the Monte Carlo simulation. The full curves represent the different contributions.

E. Monte Carlo calculations

A great deal of effort was put into the Monte Carlo program to determine accurately the detection efficiency of the apparatus for γ rays and also to eliminate events with four γ rays coming from background reactions and still present after the χ^2 cut has been applied.

1. Efficiency and resolution of the apparatus

The trigger was simulated by taking into account the geometry and the lead distribution of the veto counters B (Fig. 1). The effect of the neutron interactions giving charged products inside the target, the scintillators, and the lead was also accounted for in the calculations. Events of the type $\pi^- p \to \pi^0\pi^0 n$ were generated according to the Dürr-Pilkuhn distribution[5] with Wolf's parametrization[6]:

$$\frac{d\sigma}{d\Delta^2} \propto \frac{\Delta^2}{(\Delta^2+\mu^2)^2} F(\Delta^2),$$

$$F(\Delta^2) = \frac{1+R_N{}^2Q^2(-\mu^2)}{1+R_N{}^2Q^2(\Delta^2)},$$

where $R_N = 2.86$ GeV^{-1}, $Q(\Delta^2)$ is the momentum of the exchanged π in the neutron center of mass, M being the neutron mass,

$$Q^2(\Delta^2) = \frac{\Delta^2(4M^2+\Delta^2)}{4M^2},$$

Δ^2 is the invariant four-momentum transfer between the nucleons, and μ is the pion mass.

The events were generated according to the invariant-phase-space $\pi\pi$ mass distribution and the production of the dipion in a S wave; with these assumptions the calculated trigger efficiency was 0.49.

The detection efficiency of the spark chambers was calculated by taking into account the following effects: chamber geometry, lead thickness, angles of the tracks in the chamber, and energy loss by bremsstrahlung.

The simulation program has shown that 8% of $\pi^0\pi^0 n$ events which trigger the apparatus are seen as 4γ events in the chamber. To obtain the true weight function, all the Monte Carlo events were passed through filter and kinematical-fit programs. The variation of the weight is linear with the $\pi^0\pi^0$ mass, four times higher at 1 GeV/c than at threshold.

The parameters used later in the Chew-Low extrapolation are the $\pi^0\pi^0$ mass (ω), the neutron momentum transfer (Δ^2), and the cosine of the scattering angle ($\cos\theta^*_{\pi\pi}$). The resolutions of those parameters have been computed in the Monte Carlo program:

The $\pi^0\pi^0$ mass resolution was 40 MeV half-width at half-maximum (HWHM) near the threshold and 2

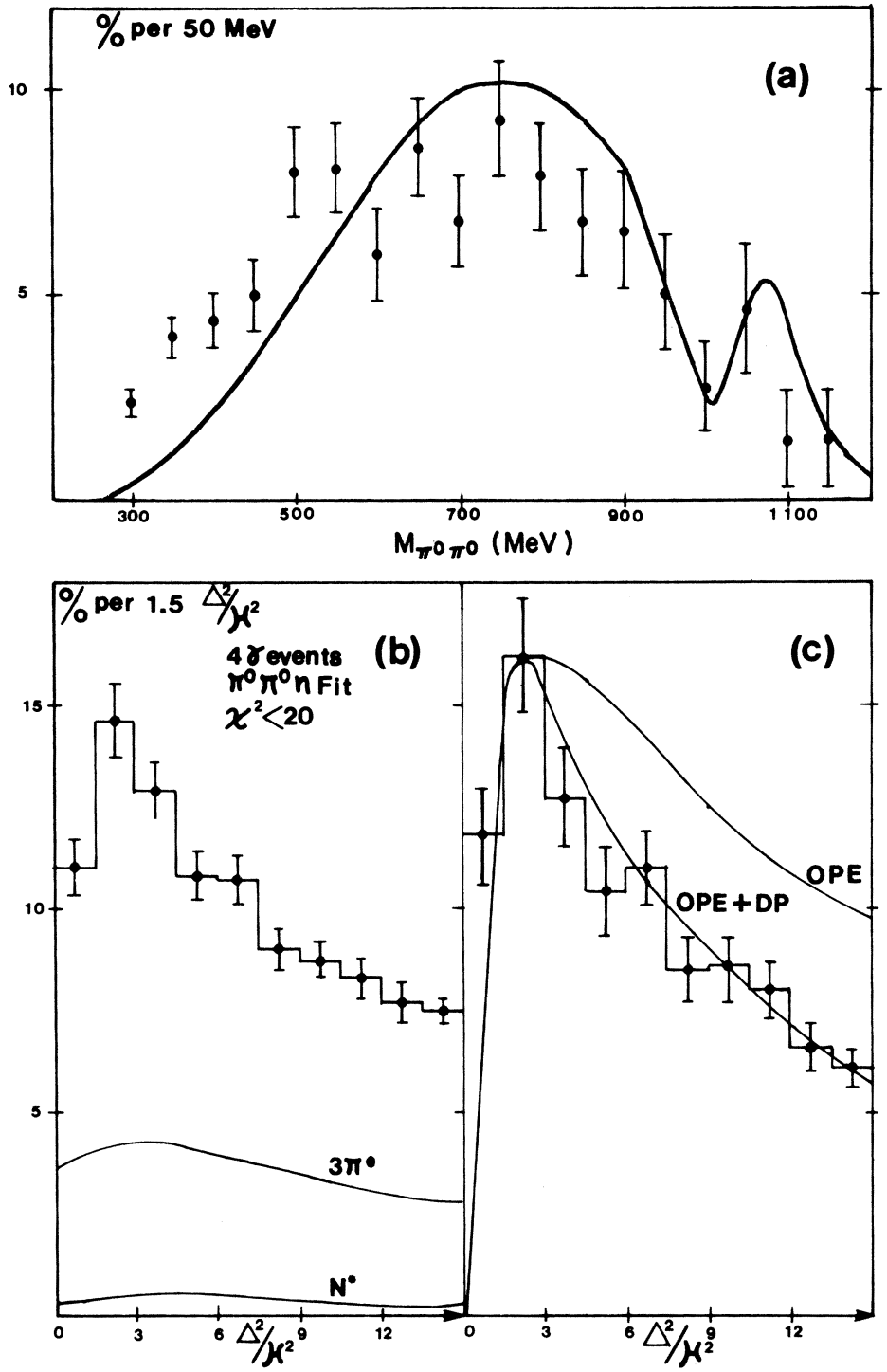

FIG. 4. (a) $\pi^\circ\pi^\circ$ invariant-mass spectrum for $\Delta^2/\mu^2 \leq 15$, corrected for detection efficiency and background. The full line represents the $\pi^\circ\pi^\circ$ mass spectrum as calculated from CERN-Munich phase shifts (Ref. 11). (b) Uncorrected Δ^2/μ^2 momentum-transfer distribution. The curves correspond to $3\pi^0$ and N^* contributions. (c) Same as (b) but corrected for detection efficiency and background. OPE is the unmodified one-pion-exchange calculation and OPE+DP is the one-pion-exchange calculation modified as in Refs. 5, 6.

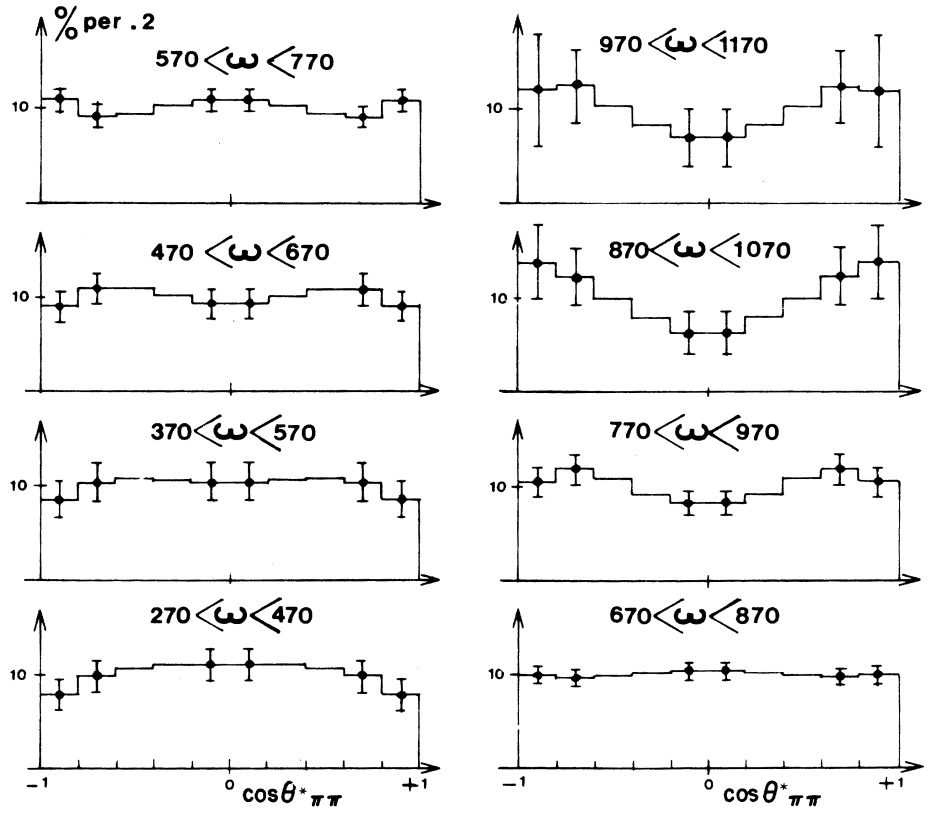

FIG. 5. cos $\theta^*_{\pi\pi}$ spectrum for various mass bins, corrected for detection efficiency and background.

times higher at $M_{\pi^0\pi^0} \simeq 1.0$ GeV.

The momentum-transfer resolution was $1.0(\Delta^2/\mu^2)$ at $\Delta_{\min}{}^2$ and reached 3.0 at $\Delta^2/\mu^2 \simeq 15.0$.

The $\cos\theta^*_{\pi\pi}$ resolution remained around 0.1 over the whole range.

2. *Contamination*

Our final data sample which fits the $\pi^0\pi^0 n$ hypothesis contains the following:

$(\pi^0\pi^0)n$ production via pion exchange,

$\pi^0 N^*$ production via ρ exchange, and

$3\pi^0 n$ and $4\pi^0 n$ events seen as four γ rays in the chamber.

The $\pi^0 N^*$ events are not eliminated by the χ^2 cut because they are real $\pi^0\pi^0 n$ events. If they are present in our data sample we should see an effect in the $(\pi^0 N)$ mass spectrum.

The $3\pi^0 n$ and $4\pi^0 n$ events with only four γ rays seen in the chamber are always present in the data, whatever χ^2 cut we apply. This is due to the fact the momentum accuracy is too poor to permit the elimination of some configurations of events where low-energy γ rays have not been seen in the chamber. The above Monte Carlo program has been used to evaluate the contamination due to the $3\pi^0$ and $4\pi^0$ events and to estimate the amount of N^* production.

$N^*(1236)$ was generated with the distribution given by Ref. 7 and with the mass distribution and decay properties given by Jackson.[8] The experimental $\pi^0 N$ mass spectrum [Fig. 3(a)] shows that the effect of the N^* production is small. The geometry of the anticounters B (Fig. 1) did not favor the trigger on the reaction $\pi^- p \to \pi^0 N^*$ because the π^0 of $N^* \to \pi^0 n$ is generally of low energy and produced at a large angle; the π^0-decay γ rays were therefore mostly emitted outside the useful solid angle of the chamber. After the χ^2 and Δ^2/μ^2 cuts only 2% of the experimental events can be explained by N^* production, which is in agreement with a total cross section of 200 μb as found by Clegg.[9]

The $3\pi^0 n$ events were generated according to η production and decay (220 μb) in addition to a background having the characteristics of the invariant phase space (450 μb).[10] For $4\pi^0 n$, only phase-space behavior was used (150 μb).[10] We have found that 26% of the experimental four-γ-ray events came from these reactions where only four γ rays were converted. The main effect of these

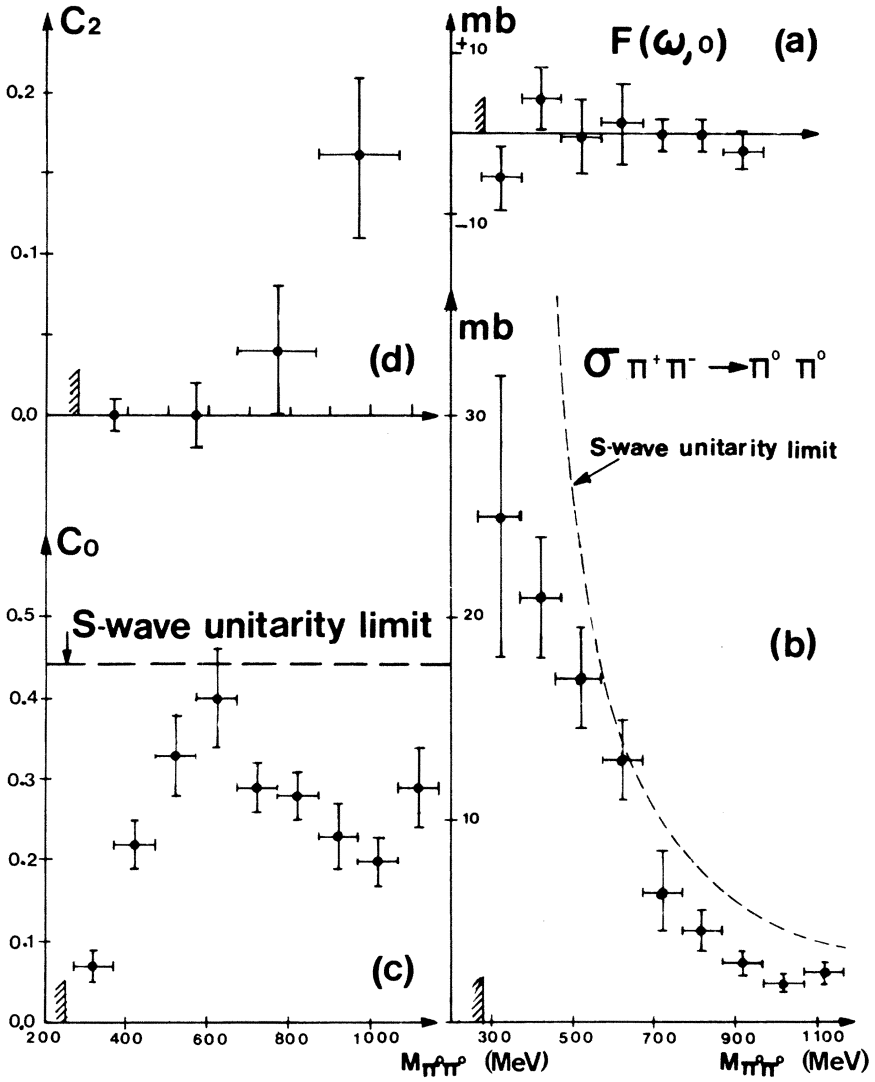

FIG. 6. (a) $F(\omega,\Delta^2)$ for $\Delta^2/\mu^2=0$, vs dipion mass, (b) extrapolated cross section of $\pi^+\pi^- \to \pi^0\pi^0$ with the constraint at $\Delta^2/\mu^2=0$, vs dipion mass, (c) variation of $C_0=\sigma(\pi^+\pi^- \to \pi^0\pi^0/2\pi\chi^2$, (d) variation of C_2 vs dipion mass.

background events is a deformation of the mass spectrum near threshold. Although this contamination is large we think that we understand it fairly well. Figure 3(b) shows that the experimental $3\pi^0$ mass spectrum for 6γ events, fitted with the hypothesis $\pi^- p \to 3\pi^0 n$, is in agreement with the Monte Carlo predictions. Another way to check the accuracy of the Monte Carlo calculations was to make a 4γ sample by removing two γ rays in 15 different possible ways from the 6γ sample. This was done simultaneously for the Monte Carlo and experimental data and the results were similar. The good description by our Monte Carlo simulations of the 2γ and 6γ samples, in which known cross sections and decays of $\pi^0 \to 2\gamma$, $\eta^0 \to 2\gamma$, $3\pi^0$ can be used as checks, allows us to be confident of the Monte Carlo data for the 4γ sample.

F. Experimental results

Figure 4(a) shows the corrected $\pi^0\pi^0$ mass spectrum for events with $\Delta^2/\mu^2<15$. On this figure the full line represents the $\pi^0\pi^0$ mass spectrum calculated with the Chew-Low formula using CERN-Munich phase shifts (down solution).[11] The major differences are just above threshold and around 800 MeV. The same differences are also found in a phase-shift analysis using our $\pi^0\pi^0$ results.[12] Figures 4(b) and 4(c) display the momentum-transfer distributions before and after the corrections.

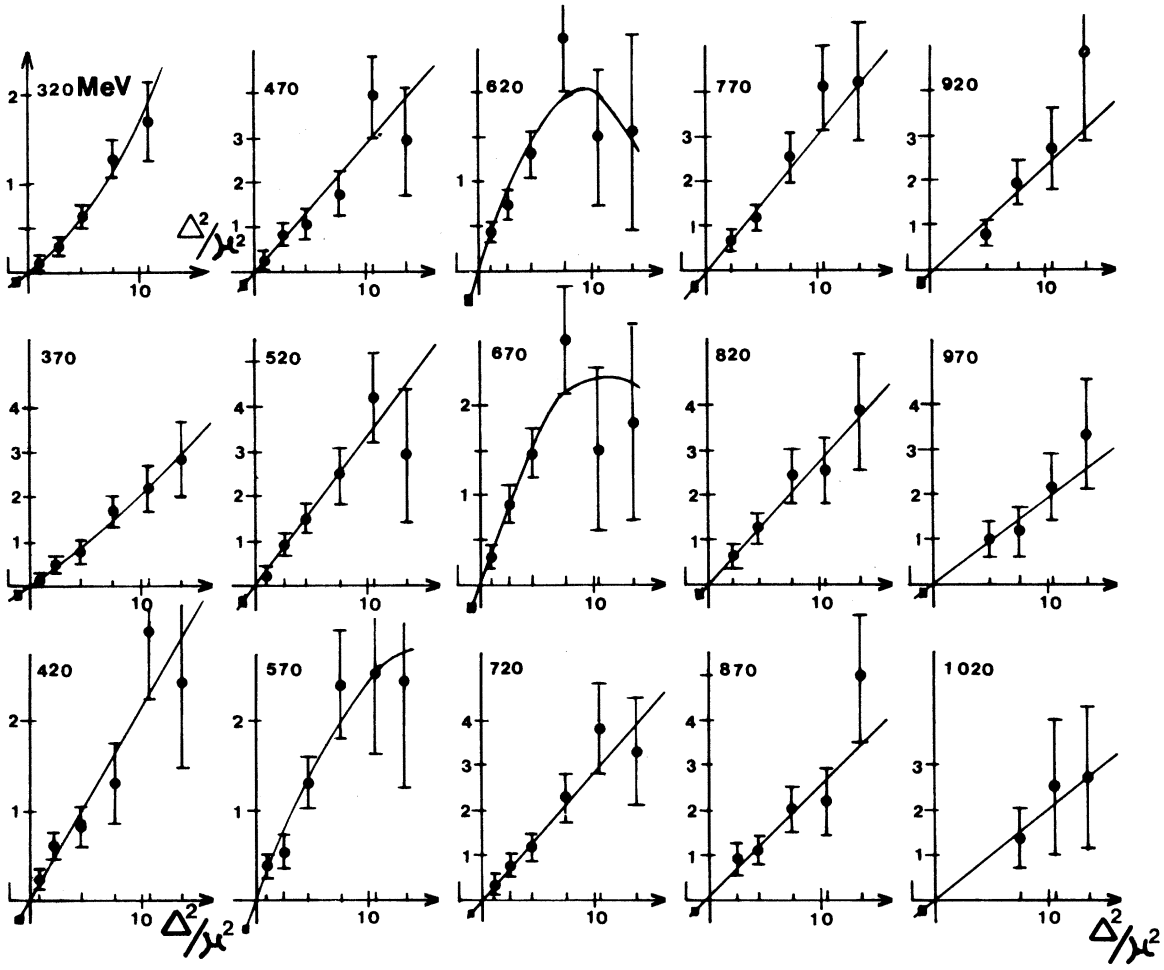

FIG. 7. Extrapolation curves giving C_0 for various dipion mass bins.

It should be observed that the experimental Δ^2/μ^2 distribution is characterized by a peak at low Δ^2/μ^2. This is typical of one-pion-exchange (OPE) peripheral reactions. On the contrary, the same distributions for background reactions have a moderate slope.

The $2\pi^0$ cross section for $\Delta^2/\mu^2 < 15$ is found to be 701 ± 55 μb. But this value is affected by a systematic error of 18% mainly due to uncertainties on background cross sections (12%) and to an uncertainty (6%) coming from the estimation of the weight function.

Figure 5 shows the $\pi^0\pi^0$ angular distributions (i.e., the cosine of the direction of the scattered π^0 relative to the incident π^- in the rest frame of the dipion mass). Up to 850 MeV of $\pi^0\pi^0$ effective mass, the angular distribution is isotropic; above 850 MeV an effect due to the D wave appears.

IV. CHEW-LOW EXTRAPOLATION

We obtained 2295 $\pi^0\pi^0$ events at low-momentum transfer and $\chi^2 < 20$ ($\Delta^2/\mu^2 < 15$). We used them to perform Chew-Low extrapolation in order to obtain the total $\pi^+\pi^- \to \pi^0\pi^0$ cross section and the C_0 and C_2 coefficients of a Legendre polynomial expansion of $d\sigma/d\Omega$.

We define the usual[13] off-shell differential cross section for $\pi\pi$ scattering by

$$F(\omega, \Delta^2) = \frac{\pi}{f^2} \frac{k_{\text{lab}}^2}{\omega(\omega^2/4 - \mu^2)^{1/2}} (\Delta^2 + \mu^2)^2 \frac{d^2\sigma}{d\Delta^2 d\omega^2},$$

where $f^2 = 0.081 \pm 0.002$ is the πN coupling constant, ω is the $\pi^0\pi^0$ mass, and k is the incident-pion laboratory momentum. This function extrapolated to $\Delta^2/\mu^2 = -1$ gives the total cross section for the reaction $\pi^+\pi^- \to \pi^0\pi^0$.

We divided the Chew-Low plot into cells of $\omega \times (\Delta^2/\mu^2) = 100.0$ MeV $\times 1.5$ for $0.0 \leq \Delta^2/\mu^2 < 3.0$ and into cells of $\omega \times (\Delta^2/\mu^2) = 100.0$ MeV $\times 3.0$ for $3.0 < \Delta^2/\mu^2 < 15.0$. In each cell we have computed the function $F(\omega, \Delta^2)$ and we have expanded it according to the formula

TABLE I. Comparison of different experiments giving $\sigma_{\pi^+\pi^- \to \pi^0\pi^0}$. The abbreviations used for experimental techniques are: SC, spark chamber, DBC, deuterium bubble chamber, LHBC, liquid hydrogen bubble chamber.

						γ-ray detection			Nucleon detection					
Reference	$P_{\pi_{lab}}$ (GeV/c)	Number of events	Technique	Rad. length	$\Delta\Omega_{lab}$ (sr)	γ multiplicity used	$\Delta\theta\gamma$ (msr)	$\frac{\Delta P_\gamma}{P_\gamma}$ (%)	Efficiency	$\Delta\Omega_{lab}$ (sr)	$\Delta\theta_n$ (msr)	$\frac{\Delta P_n}{P_n}$	N^* found	Calculation of $\sigma_{\pi\pi}$
Corbett *et al.* (Ref. 16)	1.715 to 2.46	≃1200	SC	2.3	10.5	only 4γ	10						Yes	Form factor
Sonderegger *et al.* (Ref. 18)	2.55 to 5.75	≃3000	SC	11.5	1.0	only 4γ	15	≳30.0					No	Form factor
Shibata *et al.* (Ref. 19)	10.0	547	SC	5.0	0.25	only 4γ	10						No	Form factor
This experiment	2.1	2295	SC	1.9	5.0	only 4γ	20	15.0					No	Constrained extrapolation
Deinet *et al.* (Ref. 23)	1.77	4988	SC + n counters	4.0	10.0	1 to 4			≃10%	0.2	30	≃3%	No	Constrained extrapolation
Skuja *et al.* (Ref. 15)	1.6 to 2.4	1323	SC + n counters	7.0	10.5	only 4γ	20	≳40.0	20%	0.04	30	≃3%	Yes	Form factor
Braun *et al.* (Ref. 22)	2.15	197	DBC	1.5	≃2.5	2 to 4	≃5	≳30.0	≃80%	≲4π	5	1.5 to 25.0	No	Form factor
Bensinger *et al.* (Ref. 21)	2.15	748	DBC	1.5	≃2.5	2 to 4	≃5	≳30.0	≃80%	≲4π	5	1.5 to 25.0	No	Form factor
Grivaz *et al.* (Ref. 20)	3.5	464	LHBC	1.5	10.0	4γ	5	20.0	80%	≲4π	5	1.5 to 2.5		OPE in physical region

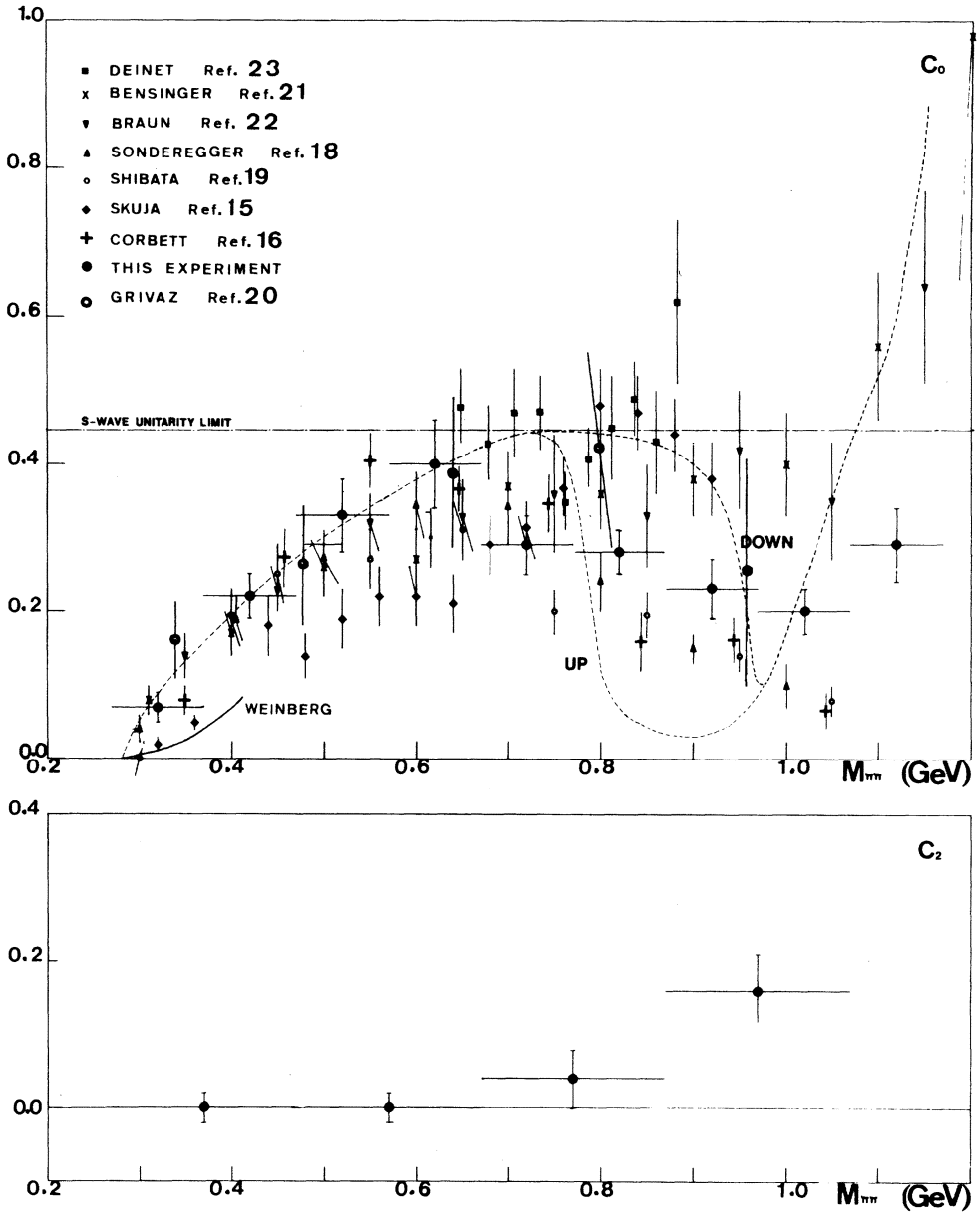

FIG. 8. $C_0(\pi^+\pi^- \to \pi^0\pi^0)$ data from this experiment and from others. The solid curve shows Weinberg's scattering-length prediction (Ref. 17). The dashed curves show the phase-shift-analysis prediction for up and down solutions (Ref. 12).

$$F(\omega, \Delta^2) = 2\pi\bar{\lambda}^2 \sum_{i=0}^{n} a_i(\omega)\left(\frac{\Delta^2}{\mu^2}\right)^i$$

with $n \leq 2$.

The extrapolated value of the function $F(\omega, \Delta^2)$ at $\Delta^2/\mu^2 = 0$ is compatible with zero in the whole mass range [Fig. 6(a)]. This shows that the background has been truly rejected and that we are dealing mainly with an OPE process having an $N\pi N$ vertex. This leads us to expand the formula $F(\omega, \Delta^2)$ as

$$F(\omega, \Delta^2) = 2\pi\bar{\lambda}^2 \sum_{i=1}^{n} b_i(\omega)\left(\frac{\Delta^2}{\mu^2}\right)^i$$

without a constant term.

The extrapolation to $\Delta^2/\mu^2 = -1$ of this function gives a more accurate determination of $\sigma_{\pi\pi}$ than the previous one. Figure 7 shows these extrapolations after multiplication by $1/2\pi\bar{\lambda}^2$, which yields the C_0 coefficient [$\sigma_{\pi\pi}(\omega) = 2\pi\bar{\lambda}^2 C_0(\omega)$, $\bar{\lambda} = \hbar c/q$, $q^2 = \omega^2/4 - \mu^2$]. The variation of $\sigma_{\pi\pi}$ and C_0 vs ω are shown, respectively, in Figs. 6(b) and 6(c).

In order to estimate possible effects due to the binning, we have also used different cells in $\omega \times (\Delta^2/\mu^2)$; the values of C_0 obtained with the different sets of cells were always compatible. We have checked the effect of the background subtraction (mainly $3\pi^0 N$ reaction) by varying the σ_{tot} and $d\sigma/d\Delta^2$ of this background within the limits of the experimental errors[9,10]: Changes in $d\sigma/d\Delta^2$ had almost no effect because the background slope in Δ^2 is always moderate compared with the experimental slope. Changes in σ_{tot} did not vary considerably the general behavior of C_0 vs ω (the variation of the absolute value is continuous); the maximum variation (less than 15%) appears at low mass and is negligible at $\omega = 1.0$ GeV.

In order to obtain the C_2 coefficients, we first expanded the following function in terms of Legendre polynomial:

$$F(\omega, \Delta^2, \cos\theta^*) = \frac{\pi}{f^2} \frac{k_{1ab}^2}{\omega(\omega^2/4 - \mu^2)^{1/2}} (\Delta^2 + \mu^2) \frac{d^3\sigma}{d\Delta^2 d\omega^2 d\cos\theta^*} = \pi\lambda^2 [C_0(\omega, \Delta^2) + C_2(\omega, \Delta^2) P_2(\cos\theta)],$$

where θ is the $\pi\pi$ scattering angle in the dipion rest frame.

We chose to divide the Chew-Low plot in cells of $\omega \times \cos\theta^*_{\pi\pi} \times (\Delta^2/\mu^2) = 200.0$ MeV $\times 0.2 \times 3.0$ for $\Delta^2/\mu^2 < 6.0$ and 200.0 MeV $\times 0.2 \times 4.5$ for $\Delta^2/\mu^2 > 6.0$ in order to account for the lower statistics in the high-(Δ^2/μ^2) region. The two coefficients were extrapolated to $\Delta^2/\mu^2 = -1.0$, using $C(\omega, \Delta^2/\mu^2) = c' \times (\Delta^2/\mu^2)$. The values found from this method for C_0 are in agreement with the previous ones coming from the σ_{tot} extrapolation but the errors are larger.

The variation of C_2 vs ω is shown in Fig. 6(d). The variation of C_0 vs ω presents a rapid rise between threshold and 670 MeV, where it reaches the S-wave unitarity limit; above 670 MeV it decreases up to $\omega = 1000$ MeV and then rises again. C_2 is consistent with zero for $\omega < 850$ MeV and then rises; hence D-wave effects in $\pi^+\pi^- \to \pi^0\pi^0$ are not strong enough to be visible under 850 MeV.

V. COMPARISON WITH OTHER EXPERIMENTAL RESULTS

The present comparison is restricted to the experiments where values of $\sigma_{\pi^+\pi^- \to \pi^0\pi^0}$ have been explicitly given. This is not the case for Apel *et al.*,[14] who compare published $\pi\pi$ phase shifts with results from an analysis in the physical region.

Table I shows the main characteristics of these experiments, and Fig. 8 displays the corresponding variation of C_0 vs ω. For the energy range between threshold and 620 MeV, all the results are in agreement except for Skuja[15] and Corbett[16]; for the latter it seems that a change of factor 2.7 in the normalization would restore the agreement. This factor has been applied on Fig. 8. The rapid rise at threshold does not seem to be compatible with Weinberg's scattering-length predictions.[17]

Above 620 MeV it appears that for a given experimental technique the behavior of the C_0 is similar. Corbett renormalized, Sonderegger,[18] Shibata,[19] and our results (spark chambers) give a $\sigma_{\pi\pi}$ which decreases up to $\omega = 1000$ MeV. In absolute value the measurements are compatible within the errors. Grivaz[20] (heavy-liquid bubble chamber) is also compatible with this behavior. Bensinger[21] and Braun[22] (D^2 bubble chamber) are in very good agreement with each other. Contrary to the other experiments they give a C_0 which increases continuously with energy. Deinet[23] and Skuja[15] who both detected the neutron are in disagreement except in the 800-MeV region, where they reach the S-wave unitarity limit; in this region they give values of C_0 higher than all the other experiments.

VI. COMPARISON WITH PHASE-SHIFT-ANALYSIS PREDICTIONS

Many phase-shift analyses[11,24,25] have been performed but none of them used the $\pi^+\pi^- \to \pi^0\pi^0$ results. These analyses suffer always from an ambiguity in the determination of the S_0 wave between 650–950 MeV of $\pi\pi$ mass. The C_0 coefficients computed from these analyses $[C_0 = \frac{4}{9} \sin^2(\delta_{S_0} - \delta_{S_2})]$ have very different behaviors. In particular a simultaneous analysis of the 3 final states $(\pi^+\pi^+, \pi^-\pi^0, \pi^+\pi^-)$ (Ref. 12) gives 2 statistically equivalent solutions (called up and down) for the S_0 wave which predict the 2 behaviors of C_0 shown on Fig. 8. For the full mass range none of the measured C_0 is in agreement with those predictions. The numerous checks that we have done on our data give us sufficient confidence to use them as input in a phase-shift analysis of the 4 measurable channels of the $\pi\pi$ elastic scattering.[12]

---

[1]G. Villet, M. David, R. Ayed, P. Bareyre, P. Borgeaud, J. Ernwein, J. Feltesse, Y. Lemoigne, P. Marty, and A. V. Stirling, in *π-π Scattering—1973*, proceedings of the International Conference on π-π Scattering and Associated Topics, Tallahassee, 1973, edited by P. K. Williams and V. Hagopian (AIP, New York, 1973); and work cited by G. Laurens, in Proceedings of the Second International Conference on Elementary Particles,

Aix-en-Provenie, 1973 [J. Phys. (Paris) Suppl. 34, C1-217 (1973)].
[2]A. Dillet, M. Goldwasser, J. C. Michau, J. Mullie, B. Pichard, and G. Riols, proceedings of the International Conference on Data Handlings Systems in High-Energy Physics, Cambridge, 1970 (unpublished).
[3]W. Heitler, *The Quantum Theory of Radiation* (Clarendon, Oxford, 1936).
[4]B. Degrange, thesis, Univ. of Paris, 1970 (unpublished).
[5]H. P. Dürr and H. Pilkuhn, Nuovo Cimento 40, 899 (1965).
[6]G. Wolf, Phys. Rev. Lett. 19, 925 (1967); and Phys. Rev. 182, 1538 (1969).
[7]G. Gidal, G. Borreani, D. Grether, F. Lott, R. W. Birge, S. Y. Fung, W. Jackson, and R. Poe, Phys. Rev. Lett. 23, 994 (1969).
[8]J. D. Jackson and K. Gottfried, Nuovo Cimento 33, 309 (1964).
[9]R. B. Clegg, Nucl. Phys. B6, 75 (1968).
[10]H. R. Crouch, Jr., R. Hargraves, R. E. Lanou, Jr., J. T. Massimo, A. E. Pifer, A. M. Shapiro, M. Widgoff, A. E. Brenner, M. Ioffredo, F. D. Rudnick, G. Calvelli, F. Gasparini, L. Guerriero, G. A. Salandin, A. Tomasin, C. Voci, F. Waldner, Y. Eisenberg, E. E. Ronat, S. Toaff, P. Bastien, B. Brabson, B. T. Feld, V. Kistiaskowski, Y. Goldschmidt-Clermont, D. Miller, I. A. Pless, A. Rogers, L. Rosenson, L. Ventura, T. L. Watts and R. K. Yamamoto, Phys. Rev. Lett. 21, 845 (1968).
[11]G. Grayer, B. Hyams, C. Jones, P. Schlein, W. Blum, H. Dietl, W. Koch, E. Lorenz, G. Lütjens, W. Manner, J. Meissburger, W. Ochs, U. Stierlin, and P. Weilhammer, in *Experimental Meson Spectroscopy—1972*, proceedings of the Third International Conference, Philadelphia, edited by A. H. Rosenfeld and K.-W. Lai (AIP, New York, 1972), p. 5.
[12]G. Villet, M. David, R. Ayed, P. Bareyre, P. Borgeaud, J. Ernwein, J. Feltesse, and Y. Lemoigne, CEN Internal Report No. DPhPE 76-09 (unpublished).
[13]J. Naisse and J. Reignier, Fortschr. Phys. 12, 523 (1964).
[14]W. D. Apel, J. S. Ausländer, H. Müller, G. Sigurdsson, H. M. Staudenmaier, U. Stier, E. Bertolucci, I. Mannelli, G. Pierazzini, P. Renak, A. Scribano, F. Sergiampietri, and M. L. Vincelli, Phys. Lett. 41B, 542 (1972).
[15]A. Skuja, M. A. Wahlig, T. B. Risser, M. Pripstein, J. E. Nelson, J. R. Linscott, R. W. Kenney, O. I. Dahl, and R. B. Chaffee, Phys. Rev. Lett. 31, 653 (1973).
[16]I. F. Corbett, C. J. S. Damerell, N. Middlemas, D. Newton, A. B. Clegg, W. S. C. Williams, and A. S. Carroll, Phys. Rev. 156, 1451 (1967).
[17]S. Weinberg, Phys. Rev. Lett. 17, 616 (1966).
[18]P. Sonderegger and P. Bonamy, *Proceedings of the Fifth International Conference on Elementary Particles, Lund*, 1969, edited by G. von Dardel (Berlingska, Boktryckeriet, Lund, Sweden, 1970).
[19]E. I. Shibata, D. H. Frisch, and M. A. Wahlig, Phys. Rev. Lett. 25, 1227 (1970).
[20]J. F. Grivaz, P. Davis, D. Fournier, J. Y. Grandpeix, J. J. Veillet, A. Halsteinslid, E. Lillestol, K. Myklebost, G. Irwin, F. Jacquet, and P. Mine, Phys. Lett. 61B, 400 (1976).
[21]J. R. Bensinger, A. R. Erwin, M. A. Thompson and W. D. Walker, Phys. Lett. 36B, 134 (1971).
[22]K. J. Braun, D. Cline, and V. Scherer, Phys. Rev. Lett. 21, 1275 (1968).
[23]W. Deinet, A. Menzione, H. Müller, H. M. Staudenmaier, S. Buniatov, and D. Schmitt, Phys. Lett. 30B, 359 (1969).
[24]G. Laurens, thesis, Univ. of Paris [CEA Report No. CEA-N-1497, 1971 (unpublished)]; J. P. Baton, G. Laurens, and J. Reignier, Phys. Lett. 33B, 528 (1970).
[25]S. D. Protopopescu, M. Alston-Garnjost, A. Barbaro-Galtieri, S. M. Flatte, J. H. Friedman, T. A. Lasinski, C. R. Lynch, M. S. Rabin, and F. T. Solmitz, Phys. Rev. D 7, 1279 (1973).